Reports in Mechanical Engineering
Vol. 7, No. 1, 2026, pp. 199-214
ISSN: 2683-5894, DOI: https://doi.org/10.31181/rme558

Model of Contact Temperature Fields in a Composite Cylinder of a Modernized Locomotive Frame

Galina Khromova[1], Davran Radjibaev[1], Jingyong Zhang[2], Aliya Zabiyeva[3*], Kyrmyzy Balabekova[3*], Assylbek Kassenov [4,5], Umida Ziyamukhamedova[1], Ravshanbek Mirsaatov[1], Zhou Fei[6]

[1] Faculty of Railway Transport Engineering, Tashkent State Transport University, Tashkent 100176, Uzbekistan
[2] School of Material and Physics, China University of Mining and Technology, Jiangsu, Xuzhou 221116, China
[3] Faculty of Transport and Energy, Eurasian National University, Astana, Kazakhstan
[4] Toraighyrov University, Pavlodar, Kazakhstan
[5] Kazakh National University of Water Management and Irrigation, Taraz 080000, Kazakhstan
[6] PRD office, Shinawarta Univ*ersity*

Article Info

Article history:

Received December 19, 2025
Revised March 17, 2026
Accepted March 29, 2026

Keywords:

Electric Locomotive,
Main Frame of the Electric Locomotive Body,
Dynamic Loads,
Stress-Strain State of the Main Frames of Electric Locomotives,
Contact Temperature Fields in a Composite Cylinder,
Reinforcing Steel Plates,
Fatigue Safety Factor,
Overhaul of the Main Frames of Electric Locomotives,
Algorithm

ABSTRACT

The reliability and durability of electric locomotive frames are strongly influenced by coupled thermomechanical effects arising during structural modernization, particularly due to welding-induced temperature gradients and operational dynamic loads. However, existing studies on composite cylindrical structures typically address thermal contact or mechanical loading separately, limiting their applicability to real conditions.This study proposes a unified numerical–analytical framework for the coupled analysis of contact temperature fields and the stress–strain state in composite cylindrical elements of modernized locomotive frames (VL80s series). The approach integrates three-dimensional heat conduction with spatial elasticity theory, enabling simultaneous consideration of welding-induced thermal effects and dynamic loading. The governing boundary value problems are solved using Fourier–Bessel series expansions, Laplace transforms, and iterative piecewise linear approximation. The model is calibrated using experimental data obtained from full-scale locomotive tests and validated against finite element simulations (SolidWorks). The results demonstrate high predictive accuracy, with deviations from experimental measurements within 3–10%. Structural reinforcement by welded plates reduces peak stresses in critical zones by 10–15%, while maintaining safety factors above regulatory limits (≥1.4), even under material aging conditions. The influence of thermal contact stresses is shown to be moderate but essential for accurate durability assessment. The main contribution of this work lies in the development of an experimentally validated coupled thermomechanical model and an efficient engineering-oriented computational algorithm for composite cylindrical structures under combined loading conditions. The proposed methodology provides a reliable tool for the design, modernization, and residual life assessment of locomotive frames and can be extended to other transport and mechanical systems operating under similar thermomechanical environments.

Corresponding Author:

Aliya Zabiyeva
Faculty of Transport and Energy, Eurasian National University, Astana, Kazakhstan
Email: zabiyeva_ab@enu.kz
Kyrmyzy Balabekova
Faculty of Transport and Energy, Eurasian National University, Astana, Kazakhstan
Email: balabekova_kg@enu.kz

1. Introduction

The reliability, durability, and safety of electric locomotive structures are critical factors in modern railway

transport systems, particularly under increasing operational loads and extended service life requirements. In practice, one of the most effective approaches to prolonging the operational lifespan of locomotives is the modernization of their main load-bearing structures, including the installation of reinforcing steel plates in zones prone to fatigue damage. However, such processes of modernisation, especially those involving welding, introduce complex thermomechanical effects that significantly influence the stress–strain state of the structure.

Until now, the issue of the influence of thermal contact processes occurring in the frames of locomotives has been practically ignored due to the complexity of the resulting tasks and the presence of many variable external factors leading to complex boundary conditions. However, taking into account the temperature effects on the details of the frame of a spatial structure can significantly adjust its power and performance characteristics and will make it possible to purposefully create reliable modernized structures of increased strength for the conditions of the sharply continental climate of Central Asia and Kazakhstan.

During welding, non-uniform heating and cooling generate contact temperature fields, residual stresses, and local material deformations. These effects are further compounded by dynamic loads arising during locomotive operation, including vibrations, traction forces, and track-induced irregularities. As a result, the accurate assessment of the combined influence of thermal and mechanical factors becomes essential for ensuring structural integrity and predicting the remaining service life of locomotive frames.

Before making predictions about the thermal conductivity of the contact at the docking boundaries of a straight cylindrical rod composed of two parts, it is necessary to make a brief review of the scientific studies made on classical studies in this area, and it is also necessary to have an adequate understanding of the mechanical and thermal processes that affect the stress-strain state of the electric locomotive frames and its component parts and assemblies.

In general, contact studies on the stress-strain state for cylindrical surfaces are divided into two groups, with the first group devoted mainly to the development of theory, dealing mainly with fundamental issues, and the second group, based on experimental studies and classified as applied research (S. Wahid & C. Madhusudana, 2000).

A substantial body of research has been devoted to the analysis of heat transfer and stress–strain behavior in cylindrical and composite structures. Classical studies in the field of heat conduction in composite cylinders have established theoretical foundations for modeling thermal contact resistance and temperature distribution under simplified conditions. These models typically assume axisymmetric heat flow and idealized boundary conditions. At the same time, research in elasticity theory has addressed stress concentrations and deformation behavior in heterogeneous cylindrical bodies subjected to mechanical loading.

Wahid, S. M. S., and Madhusudana, C. V. (S. Wahid & C. Madhusudana, 2000) analyzed theoretical and experimental studies on heat transfer in composite cylinders, classifying these studies as fundamental theories using idealized surfaces of complex configurations and applied studies examining the properties of specific materials and cylindrical objects. At the same time, it was noted that the application of complex mathematical models does not lead to concrete results and often does not agree with the data of experimental studies.

In general, two basic models are proposed for studying heat conduction through cylindrical contacts: composite cylindrical rods or cylindrical shells. For the most part, the heat flow through composite cylinders is assumed to be axisymmetric and radial.

Tulekov et al. (Tulekov et al., 2023) presents a predictive model of thermal contact conductivity through a cylindrical joint as a function of material properties, cylinder surface geometry and properties, and initial fit degree.

More recent studies have extended these approaches by incorporating numerical methods and computational modeling techniques, including finite element analysis, to investigate the interaction between structural components. However, most existing models consider either thermal effects or mechanical loading separately. In addition, many approaches rely on simplified assumptions that do not adequately reflect real conditions, particularly in the presence of welding-induced residual stresses and dynamic loads.

Bianchi et al. (Bianchi et al., 2025) carried out a theoretical analysis of the interaction between cylindrical tubes. Both isothermal and isothermal boundary conditions at the interface were studied. The results are presented in the form of a computer model to study the contact resistance, but this model did not take into account additional dynamic influences.

Yovanovich M. M. (Yovanovich, 2000) offer a method for predicting the conductance of cylindrical contacts based on advanced models for conductance of flat contacts that considers contact pressure, microhardness, and surface roughness. The procedure is iterative in nature, and results are presented in the form of thermal contact conductance as a function of an estimated contact pressure.

V.V. Vasiliev's monograph (Vasiliev & Morozov, 2001) presents problems of spatial theory of elasticity for applied research, including the classical problems of the theory of elasticity of cylindrical shells.

Importantly, the coupled effect of contact temperature fields and dynamic operational loading in composite

cylindrical elements of locomotive frames remains insufficiently studied. Existing works rarely integrate experimental data with analytical and numerical models, limiting their applicability for engineering practice. Furthermore, the influence of modernization measures, such as the installation of reinforcing plates, on the thermomechanical behavior of locomotive frames has not been comprehensively quantified.

To address these limitations, this study aims to develop a unified numerical–analytical framework for modeling contact temperature fields and the associated stress–strain state in composite cylindrical elements of modernized locomotive frames. The focus is placed on structures of the VL80s electric locomotive, widely used in railway systems with harsh climatic and operational conditions.

The proposed approach combines three-dimensional heat conduction modeling with spatial elasticity theory, enabling the simultaneous analysis of thermal and mechanical effects. The methodology incorporates advanced mathematical tools, including Fourier–Bessel series expansions, Laplace transforms, and iterative solution techniques, implemented in the MATHCAD 15 environment. In addition, the model is calibrated and validated using experimental data obtained from full-scale tests of locomotive frames under real operating conditions.

The main contributions of this study are as follows:

- development of a coupled thermomechanical model for composite cylindrical structures subjected to welding-induced temperature fields and dynamic loads;
- formulation of an efficient numerical–analytical solution method suitable for engineering applications;
- integration of experimental diagnostic data into the modeling framework to improve accuracy and reliability;
- quantitative assessment of the effect of structural reinforcement on stress reduction and fatigue performance;
- validation of the proposed model through comparison with finite element simulations and experimental measurements.

The results of this work provide a scientific and practical basis for improving the design, modernization, and maintenance strategies of locomotive frames, contributing to enhanced reliability, safety, and cost-effectiveness in railway transport systems.

2. Objects and Methods of Research

The objects of the study are the structural elements of the modernized frame of the locomotive type composite cylinders under external loading by static and dynamic loads, as well as under the influence of contact temperature fields arising during welding.

The research methodology includes the analysis of systems of equations in partial derivatives that describe oscillations of sections of elastic curvilinear elements of variable bending stiffness with a spatial arrangement of sections, taking into account the influence of increased speeds, the solution of which is carried out by the methods of operational Laplace calculus and the further use of iterative methods (the method of piecewise linear approximations) on a computer based on the Fourier and Bubnov-Galerkin methods, numerical studies were performed in the MathCad 15 environment. For numerical calculation programs, 2 certificates of official registration of the computer program of the Republic of Uzbekistan (No. DGU 07664, 31.04.2020 and No. DGU 10286 of 24.02.2021) were received (Bhatti & Absamatov, 2025).

The reliability of the results obtained is ensured by the use of well-known standard methods of strength of materials, dynamics and strength of machines, instruments and equipment, as well as the use of numerical methods: the Fourier method, piecewise linear approximation and the iteration method; as well as comparison of research results with known data and experimental studies.

The methodology for conducting experimental studies was determined by a set of rules for the application of standard principles for carrying out full-scale tests, which consisted of studying external and internal dynamic and temperature effects, using appropriate equipment and apparatus (vibration sensors and strain gauges), and using an automated complex for recording and processing experimental data using probabilistic-statistical methods.

The purpose of the proposed methodology of theoretical and experimental research to substantiate the process of modernization of the main frame of the VL-80 electric locomotive under operating conditions at JSC Uzbekistan Railways is to determine the maximum stresses and fatigue safety factors in the sections of the main frame of the VL-80 electric locomotive body in design modes after welding (installation) of reinforcing plates.

Currently, nine sections of 3VL-80s electric locomotives have been modernized using the proposed methodology. For example, the figure (Fig. 1) shows the modernization of unit 1 of the main frame bracket reinforcement of a VL-80 electric locomotive body with the installation of reinforcing plates, completed at Ukrtemirmashtamir.

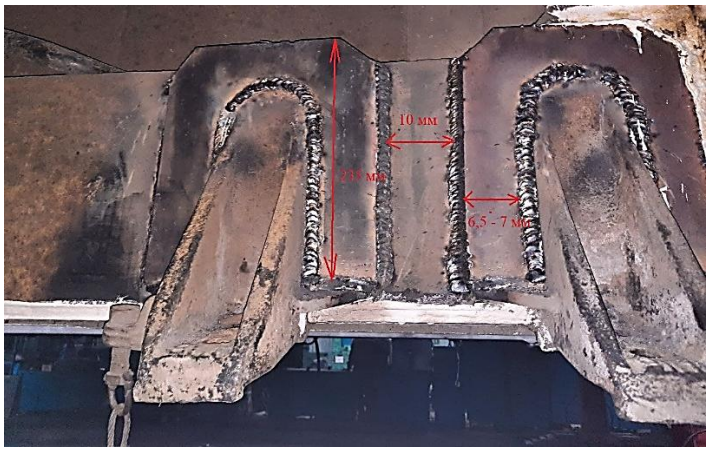

Figure 1: Modernization of Unit 1 of the Main Frame Bracket Reinforcement of the VL-80 Electric Locomotive Body with the Installation of Reinforcing Plates, Carried Out At The Ukrtemirmashtamir Unitary Enterprise.

When upgrading a locomotive frame to extend its useful life, reinforcing steel plates are welded at the points of fatigue cracking. The heating and melting of the metal during welding creates internal stresses in the metal and its deformation caused by the following:

- uneven heating and temperature distribution over the cross-section and length of the welded joint;
- casting shrinkage of the weld metal;
- structural changes in the metal during cooling.

These welding stresses and strains are intrinsic or residual stresses and strains of the metal, since they do not depend on the application of external forces to it, but appear as a result of internal forces arising from welding (Zhang et al., 2023).

In the proposed article two problems are considered for the model of force and temperature loading of the structural element of the composite cylinder type for the modernized frame of a locomotive:

Problem 1 is the main problem for a rectangular cylindrical rod composed of two parts connected at the ends.

Consider the axial tension of a composite rod whose two parts, made of different materials, are hard joined at the ends (Fig. 2). In distinction from the deformation of a monotonous body, when the corresponding stress state is determined elementary, a stress concentration arises in the contact zone of two materials with different values of elastic constants.

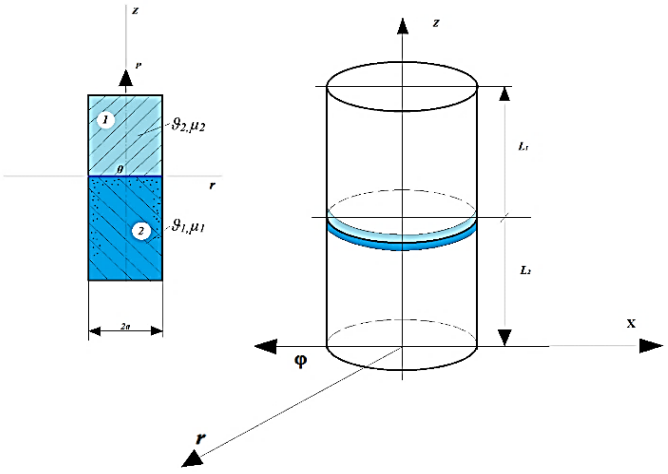

Figure 2: Calculation Scheme for a Straight-Axis Cylindrical Rod Made of Two Parts, Docked at the Ends, for a Modernized Locomotive Frame.

Studying it requires solving a spatial problem of elasticity theory with the following boundary conditions

$$\sigma_r = 0, \tau_{rz} = 0 \text{ at } r = a, -\infty < z < \infty. \quad (1)$$

$$\text{At } z \to \pm\infty \;\; \sigma_z \to P_0 = \frac{P}{F},$$

and all other components of the stress tensor are zero; P is the normal force, F is the cross-sectional area of the rod.

We accept the following assumption: we represent the lower and upper cylinders as semi-infinite. For each of them in this case it is necessary to set and solve two practical problems in stresses

$$\sigma_z = p_0 + p(r), \tau_{rz} = q(r) \text{ at } z = 0, 0 \le r \le a; \tag{2}$$

$\sigma_z = 0, \tau_{rz} = 0$ at $r = a$; $0 \le z < \infty$ -for lower cylinder;
$-\infty < z \le 0$ - for upper cylinder.

The functions *p(r)* and *q(r)* in combination with the known value p_0 determine the contact stresses. Since the component p_0 associated with the normal force P is singled out in the normal contact stresses, *p(r)* must satisfy the condition

$$\int_0^a p(r) r dr = 0. \tag{3}$$

To find *p(r)* and *q(r)*, it is necessary to use the joint displacement conditions along the plane *z=0*

$$u_1(r) = u_2(r), \quad \omega_1(r) = \omega_2(r), \quad 0 \le r \le a. \tag{4}$$

Here *u* and *ω* are the radial and vertical components of elastic displacement belonging to the first and second semi-infinite cylinders.

The solution corresponding to condition (2) for both lower and upper cylinders should practically be the solution of the first main problem. Therefore, using the stress functions in the form of K.V. Solyanik-Krass (Sumbodo et al., 2025), we represent the stresses and displacements for the lower constituent body in the form

$$\sigma_z = g_0\tilde{\sigma}_z - 2A - \sum_{k=1}^{\infty}(C_k - \gamma_k z C_k^0)\gamma_k e^{-\gamma_k z} J_0(\gamma_k r) -$$

$$- \int_0^{\infty}\{A(\lambda)I_0(\lambda r) + A^0(\lambda)[2I_0(\lambda r) + \lambda r I_1(\lambda r)]\}\lambda \sin\lambda z d\lambda, \tag{5}$$

$$\tau_{rz} = g_0\tilde{\tau}_{rz} - \sum_{k=1}^{\infty}[C_k + (1 - \gamma_k z)C_k^0]\gamma_k e^{-\gamma_k z} J_1(\gamma_k r) +$$

$$+ \int_0^{\infty}[A(\lambda)I_1(\lambda r) + A^0(\lambda)\lambda r I_0(\lambda r)]\lambda \cos\lambda z d\lambda\,, \tag{6}$$

$$\sigma_r = g_0\tilde{\sigma}_r + A + 2(1+\nu_1)A_0 + \frac{1}{r}\sum_{k=1}^{\infty}\begin{Bmatrix}[C_k + (2 - \gamma_k z)C_k^0]\gamma_k r J_0(\gamma_k r) - \\ -[C_k + 2(1-\nu_1)C_k^0 - \gamma_k z C_k^0]\, J_1(\gamma_k r)\end{Bmatrix} e^{-\gamma_k z} +$$

$$+ \frac{1}{r}\int_0^{\infty}\left\{A(\lambda)[\lambda r I_0(\lambda r) - I_1(\lambda r)] + A^0(\lambda)\begin{bmatrix}-\lambda r I_0(\lambda r) + (\lambda r)^2 I_1(\lambda r) + \\ 2(1-\nu_1)I_1(\lambda r)\end{bmatrix}\right\} \sin\lambda z d\lambda, \tag{7}$$

$$\sigma_\varphi = g_0\tilde{\sigma}_\varphi + A + 2(1-\nu_1)A_0 +$$

$$+ \frac{1}{r}\sum_{k=1}^{\infty}\{2\nu_1 C_k{}^0\gamma_k r J_0(\gamma_k r) + [C_k + (2 - 2\nu_1 - \gamma_k z)C_k^0]\, J_1(\gamma_k r)\}e^{-\gamma_k z} +$$

$$+ \frac{1}{r}\int_0^{\infty}\{A(\lambda)I_1(\lambda r) + A^0(\lambda)[(1-2\nu_1)\lambda r I_0(\lambda r) - 2(1-\nu_1)I_1(\lambda r)]\}\sin\lambda z d\lambda, \tag{8}$$

$$u = \frac{g_0 a}{2\mu_1}\tilde{u} + \frac{r}{2\mu_1}[A + 2(1-\nu_1)A_0] + \frac{1}{2\mu_1}\sum_{k=1}^{\infty} C_k + (2 - 2\nu_1 - \gamma_k z)C_k^0]e^{-\gamma_k z} J_1(\gamma_k r) +$$

$$+ \frac{1}{2\mu_1}\int_0^{\infty}\begin{Bmatrix}A(\lambda)I_1(\lambda r) + \\ +A^0(\lambda)[\lambda r I_0(\lambda r) - 2(1-\nu_1)I_1(\lambda r)]\end{Bmatrix}\sin\lambda z d\lambda\,, \tag{9}$$

$$\omega = C_1 + \frac{g_0 a}{2\mu_1}\tilde{\omega} - \frac{z}{2\mu_1}[A + 2\nu_1 A_0] + \frac{1}{2\mu_1}\sum_{k=1}^{\infty} C_k - (1 - 2\nu_1 + \gamma_k z)C_k^0 e^{-\gamma_k z} J_0(\gamma_k r) +$$

$$+\frac{1}{2\mu_1}\int_0^\infty\{A(\lambda)I_0(\lambda r)++A^0(\lambda)[2(1-\nu_1)I_0(\lambda r)+\lambda r I_1(\lambda r)]\}\cos\lambda z d\lambda\ , \tag{10}$$

We write down the solution for the upper cylinder component similarly with the only difference that we use an exponent from the positive argument $\gamma_k z$, since the variable z in this case varies in the interval [0, -∞].

The designations adopted in formulas (5) ÷ (10) are quite traditional by analogy with the works [1÷6,10]. It is worth special mentioning only the component of the solution (5), including the multiplier g_0, which has the stress dimension. From the viewpoint of the formal solution of the first main problem for a semi-infinite cylinder this component is superfluous. However, it is necessary to eliminate possible discontinuities in the radial displacements at $r=a$ when the condition of joint displacements along the contact plane is satisfied.

Thus, as a result of fulfilling four boundary conditions for the lower cylinder, four for the upper cylinder, and two conditions for the coherence of elastic displacements along the contact plane, we obtain a system of ten equations with respect to the unknowns $A(\lambda,), A^0(\lambda), C_k, C_k^0, B(\lambda), B^0(\lambda), D_k, D_k^0, p_k, q_k$ The last two unknowns are the coefficients of the Fourier-Bessel series representing the unknown functions $p(r)$and $q(r)$

$$p(r)=\sum_{k=1}^\infty p_k J_0(\gamma_k r);\qquad q(r)=\sum_{k=1}^\infty q_k J_1(\gamma_k r). \tag{11}$$

If we consider the algebraic relations between $A(\lambda,), A^0(\lambda)$, $B(\lambda), B^0(\lambda)$, C_k, p_k и D_k, q_k the system of ten equations can be reduced to a set of six equations of the following form

$$p_k-\gamma_k C_k^0+\int_0^\infty A^0(\lambda)E_k(\lambda)\lambda\,d\lambda+g_0\int_0^\infty \varsigma^*(\lambda)\frac{E_k(\lambda)}{F_1(\lambda,a)}\lambda a d\lambda=q_k\ ;$$

$$A^0(\lambda)F_1(\lambda a)+\sum_{k=1}^\infty \gamma_k a b(\gamma_k,\lambda)J_0(\gamma_k a)\left[-\frac{p_k}{\gamma_k}+\frac{2\lambda^2}{\gamma_k^2+\lambda^2}C_k^0\right]=0;$$

$$-p_k+\gamma_k C_k^0+\int_0^\infty B^0(\lambda)E_k(\lambda)\lambda d\lambda=q_k\ , \tag{12}$$

$$B^0(\lambda)F_2(\lambda a)-\sum_{k=1}^{\infty}\gamma_k a\, b(\gamma_k,\lambda)J_0(\gamma_k a)\left[-\frac{p_k}{\gamma_k}+\frac{2\lambda^2}{{\gamma_k}^2+\lambda^2}D_k^0\right]=0$$

$$-\frac{p_k}{\gamma_k}+2(1-\nu_1)C_k^0=\omega\left[-\frac{p_k}{\gamma_k}+2(1-\nu_2)D_k^0\right];$$

$$-\frac{p_k}{\gamma_k}-(1-2\nu_1)C_k^0+\int_0^\infty A^0(\lambda)M_{1,k}(\lambda)\,d\lambda$$

$$+ag_0\int_0^\infty \varsigma^*(\lambda)\frac{E_{1,k}(\lambda)}{F_1(\lambda,a)}d\lambda=\omega\left[\frac{p_k}{\gamma_k}+\qquad\qquad+(1-2\nu_1)D_k^0\right]+\omega\int_0^\infty B^0(\lambda)M_{2,k}(\lambda)d\lambda\ ;$$

The ways of further transformations (12) are seen well enough: one can get rid of, using the first and third equations; and using the fifth equation, which is simply algebraic, one can eliminate the set of unknowns D_k^0. Let us assume the equality of Poisson's coefficients $\nu_1=\nu_2=\nu$, composing the composite cylindrical rod.

The following designations will also be used hereafter

$$a_1=1+\frac{1}{\omega};\ \beta_1=-\left[2+\frac{1-\omega}{2(1-\nu)\omega}\right]; \tag{13}$$

$$a_2=2(1-2\nu);\qquad \beta_2=2\omega+\frac{1-\omega}{2(1-\nu)}.$$

As a result, after transforming (12) with (13) we get a set of two equations

$$C_k^*=\sum_{i=1}^\infty {\Gamma_{i,k}}^{(1)}C_k^*+\sum_{i=1}^\infty {\theta_{i,k}}^{(1)}p_i^*+{\Delta_k}^{(1)} \tag{14}$$

$$p_k^*=\sum_{i=1}^{\infty}{\Gamma_{i,k}}^{(2)}C_k^*+\sum_{i=1}^{\infty}{\theta_{i,k}}^{(2)}p_i^*+{\Delta_k}^{(2)}$$

The coefficients and free terms of infinite systems (14) are represented as

$$\Gamma_{i,k}^{(1)}=\frac{1}{\alpha_1\beta_1-\alpha_2\beta_1}\int_0^\infty\left[\begin{matrix}-\beta_2\left(1+\frac{1}{\omega}\right)\frac{2\lambda^2}{\lambda^2+\gamma_i^2}\lambda a E_k(\lambda)+\\+\beta_1\frac{4\lambda^2}{\lambda^2+\gamma_i^2}\gamma_k a M_k(\lambda)\end{matrix}\right]\frac{J_0(\gamma_k a)b(\gamma_i,\lambda)}{F(\lambda a)}d\lambda;$$

$$\Gamma_{i,k}^{(2)} = \frac{1}{\alpha_1\beta_1-\alpha_2\beta_1}\int_0^\infty \begin{bmatrix} -\alpha_1 \frac{4\lambda^2}{\lambda^2+\gamma_i^2}\gamma_k a M_k(\lambda) + \\ +\alpha_2\left(1+\frac{1}{\omega}\right)\left(-\frac{2\lambda^2}{\lambda^2+\gamma_i^2}\right)\lambda a E_k(\lambda) \end{bmatrix} \frac{J_0(\gamma_k a)b(\gamma_i,\lambda)}{F(\lambda a)} d\lambda; \quad (15)$$

$$\theta_{i,k}^{(1)} = \frac{1}{\alpha_1\beta_1-\alpha_2\beta_1}\int_0^\infty \begin{Bmatrix} \beta_2\left[2-\frac{2\lambda^2}{\lambda^2+\gamma_i^2}\left(1-\frac{1}{\omega}\right)\frac{1}{2(1-\nu)}\lambda a E_k(\lambda)\right]- \\ -\beta_1\left[1+\omega+\frac{2\lambda^2(1-\omega)}{(\lambda^2+\gamma_i^2)2(1-\nu)}\gamma_k a M_k(\lambda)\right] \end{Bmatrix} \frac{J_0(\gamma_k a)b(\gamma_i,\lambda)}{F(\lambda a)} d\lambda;$$

$$\theta_{i,k}^{(2)} = \frac{1}{\alpha_1\beta_1-\alpha_2\beta_1}\int_0^\infty \begin{Bmatrix} \alpha_1\left[1+\omega+\frac{2\lambda^2(1-\omega)}{(\lambda^2+\gamma_i^2)2(1-\nu)}\gamma_k a M_k(\lambda)\right]- \\ -\alpha_2\left[2-\frac{2\lambda^2}{\lambda^2+\gamma_i^2}\left(1-\frac{1}{\omega}\right)\frac{1}{2(1-\nu)}\lambda a E_k(\lambda)\right] \end{Bmatrix} \frac{J_0(\gamma_k a)b(\gamma_i,\lambda)}{F(\lambda a)} d\lambda;$$

$$\Delta_k^{(1)} = \frac{g_0}{\alpha_1\beta_1-\alpha_2\beta_1}\int_0^\infty [\beta_2\lambda a E_k(\lambda) - \beta_1\gamma_k a M_k(\lambda)]\frac{a\varsigma^*(\lambda)J_0(\gamma_k a)}{F(\lambda a)} d\lambda;$$

$$\Delta_k^{(2)} = \frac{g_0}{\alpha_1\beta_1-\alpha_2\beta_1}\int_0^\infty [\alpha_1\gamma_k a M_k(\lambda) - \alpha_2\lambda a E_k(\lambda)]\frac{a\varsigma^*(\lambda)J_0(\gamma_k a)}{F(\lambda a)} d\lambda.$$

Thus, the solution of the problem is reduced to the minimum possible number of solutions of equations - two. They form a set of two related infinite systems of linear algebraic equations, which we solve by iterative transformations using the Simpson procedure for solving integrals in the MATHCAD 15 programming environment.

Problem 2 - the problem of heat conduction for a rectangular cylindrical rod made of two parts connected at the ends.

To solve analytically (using computer for iterations and piecewise linear approximation) in case of fixed temperature at the ends the two-dimensional heat conduction problem for any function of a point heating source using two-dimensional heat conduction equation in cylindrical coordinates - *r* and *φ*. In this case the equation according to (Vujanović et al., 2012) has the form

$$\nabla^2 T - F(T)\cdot\frac{\partial T}{\partial t} = 0\,. \quad (16)$$

For a fixed temperature at $T = T_k$. Equation (16) will take the form

$$\nabla^2 T - \frac{1}{\gamma_k^2}\cdot\frac{\partial T}{\partial t} = 0\,, \quad (17)$$

where

$$\nabla^2 T = \frac{1}{r}\cdot\frac{\partial}{\partial r}\left(r\cdot\frac{\partial T}{\partial r}\right) + \frac{1}{r^2}\cdot\frac{\partial^2 T}{\partial\varphi^2}\ . \quad (18)$$

We assume that along the length Z ($0 \le Z \le L = \frac{L_c}{2}$) the change in the temperature field (in first approximation) is insignificant, i.e. along the length of the working cylinder (cylinder) of the absorber (*OZ* axis), the process is isotropic. We obtained the Laplace equation of the form

$$\nabla^2 T = \frac{1}{r}\cdot\frac{\partial}{\partial r}\left(r\cdot\frac{\partial T}{\partial r}\right) + \frac{1}{r^2}\cdot\frac{\partial^2 T}{\partial\varphi^2} = 0, \quad (19)$$

which admits partial solutions of the type

$$T_m(r,\varphi) = \left(A\cdot r^m + \frac{B}{m}\right)\cdot(\alpha\cos m\varphi + \beta\sin m\varphi), \quad (20)$$

where *m = 0, 1, 2 ...*, and $T_0(r,\varphi) = A + B\cdot\ell n(r)$, (21)

where *A, B, α, β* - are arbitrary constants determined by the boundary conditions.

We obtain the solution of equation (19) using the Fourier method in the form

$$T_k(t,r,\varphi) = T_k(t)\cdot W_k(r)\cdot U_k(\varphi). \quad (22)$$

Substituting (22) and its derivatives into equation (19), we obtain, by dividing the variables, a system of 3 ordinary differential equations of the form

$$\frac{d^2U_k(\varphi)}{d\varphi^2} + m^2 \cdot U_k(\varphi) = 0 \text{ , (23)}$$

where $m^2 = \lambda_k^2 \cdot r^2$; $\omega_k^2 = \gamma_k^2 \cdot \lambda_k^2$;

$$\frac{1}{\gamma_k^2} \cdot \frac{dT_k(t)}{\partial t} + \lambda_k^2 \cdot T_k(t) = 0 \text{ , (24)}$$

$$\frac{d^2W_k(r)}{dr^2} + \frac{1}{r} \cdot \frac{dW_k(r)}{dr} + \lambda_k^2 \cdot T_k(t) = 0 \text{ .} \quad (25)$$

To obtain the well-known Bessel equation from equation (26), let us introduce the notation $1 - \frac{v^2}{r^2} = \lambda_k^2$, then we obtain the differential Bessel equation of the classical type in the form

$$\frac{d^2W_K(r)}{dr^2} + \frac{1}{r} \cdot \frac{dW_K(r)}{dr} + (1 - \frac{v^2}{r^2}) \cdot W_K(r) = 0, \quad (26)$$

where v is a real number; $Z_m(r)$ is a cylindrical function, provided that the solution T is bounded at $r = 0$ $Z_m(r)$ is a Bessel function of the first kind - $I_m(r)$ which is calculated by the formula

$$I_m(v) = \left(\frac{r}{2}\right)^m \cdot \sum_{k=0}^{\infty} \frac{(-1)^k}{K! \cdot \Gamma(m+k+1)} \cdot \left(\frac{r}{2}\right)^{2 \cdot K}, \quad (27)$$

provided ($|arg(r)| < \pi$).

The form of the solution of equation (23) according to (Guerrieri, 2023) is known

$$U_K(\varphi) = \alpha \cdot \cos m\varphi + \beta \cdot \sin m\varphi, \quad (28)$$

where $m^2 = \lambda_K^2 \cdot r^2$, arbitrary constants, α and β are determined from boundary conditions: $T(0, r, t) = T_{H1}$ when t > 0; $T(\varphi_{max}, r, t) = T_{H2}$ subject to change

$$0 \le \varphi \le \varphi_{max} \text{ ; } 0 \le r \le r_{max} = \frac{D}{2} \text{ .} \quad (29)$$

The boundary conditions for equation (23) have the form:

$$T(\varphi, 0, t) = T_H, \quad \text{where t > 0; } T\left(\varphi, r_{max} = \frac{D}{2}, t\right) = T_{med}$$

$$\text{subject to change} \qquad 0 \le \varphi \le \varphi_{max} \text{ ; } 0 \le r \le r_{max} = \frac{D}{2} \text{ .} \quad (30)$$

The initial condition is taken as

$$T(\varphi, r, 0) = T_{heat}(r, \varphi), \text{ (heating temperature)} \quad (31)$$

where it refers to a point heat source (e.g., that arises during welding) that creates a temperature field along the radius r and angle φ, in the form of

$$T_{heat}(r, \varphi) = T_0 \cdot \cos(m_{heat}\varphi) \cdot e^{-n_{heat} \cdot r} \text{ ,} \quad (32)$$

where the coefficients $m_{heat}$and n_{heat} are determined from experimental data.

The general solution of the equation system of equations (23)-(25) is

$$T(\varphi, r, t) = \sum_{k=1}^{\infty} T_k(t) \cdot W_k(r) \cdot U_k(\varphi) \text{ ,} \quad (33)$$

where $W_K(r) = I_m(vr)$ – Bessel function of the first order,

$v^2 = r^2 \cdot (1 - \lambda_k^2)$ – is the natural frequency of the impulse change of the temperature field in time, determined from the frequency equation of the form $U_K(\varphi) = \alpha \cos m\varphi + \beta \sin m\varphi$, and function $T_K(t)$ will have the form

$$T_K(t) = T_O \cdot \cos(m_{heat}\varphi) \cdot e^{-n_{heat} \cdot r} \cdot e^{-\omega^2 \cdot t}. \quad (34)$$

Thus, the general solution of the system of equations (23)-(25) for the two-dimensional problem of temperature field propagation in a cylindrical compound cylinder will have the following form

$$T_K(\varphi, r, t) = \sum_{k=1}^{\infty} T_{Ok} \cdot \cos(m_{heat}\varphi) \cdot e^{-n_{heat} \cdot r} \cdot e^{-\omega^2 \cdot t} \cdot I_m(vr) \cdot (\alpha \cos m\varphi + \beta \sin m\varphi), \quad (35)$$

where the coefficients α and β in equation (35) are determined by iteration method using MATHCAD 15 programming environment, we also obtain the frequency value λ_k by the frequency equation.

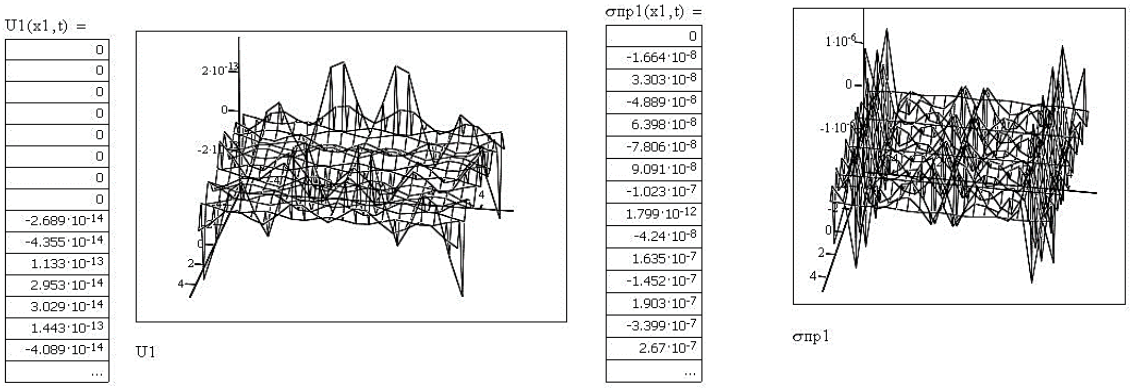

Figure 3: Volumetric Graphical Dependence of Contact Temperature Deformations and Stresses Arising in the Welded Reinforcing Plate (Steel Grade St3) On The Modernized Sidewall of the Main Frame of the Locomotive Body.

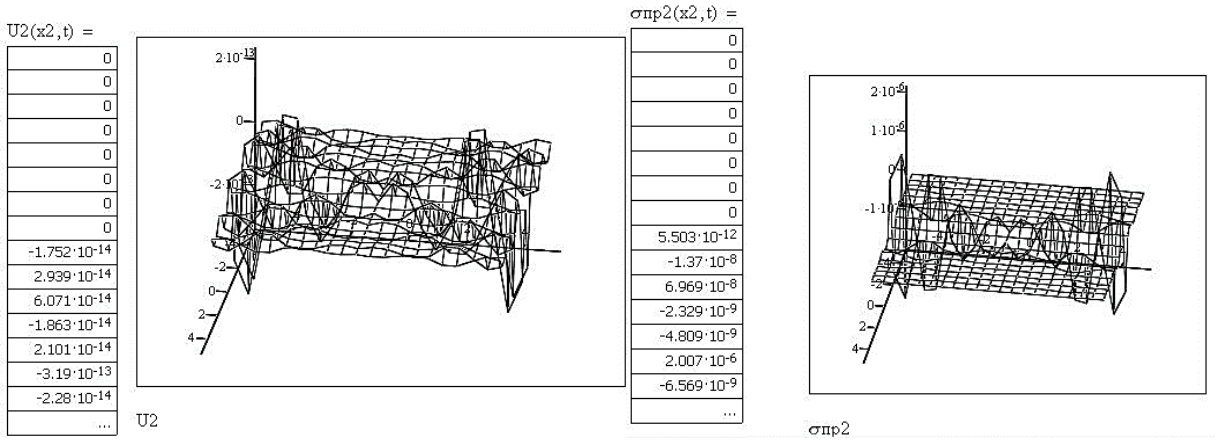

Figure 4: Volumetric Graphical Dependence of Contact Temperature Deformations and Stresses Arising in the Sidewall of the Modernized Main Frame of the Locomotive At The Installation Site of the Welded Reinforcing Plate (Steel Grade St3).

An integrated approach to modeling contact temperature deformations at the installation site of a steel reinforcing plate (grade St3 steel), welded to the modernized sidewall of the main frame of a locomotive body, using a three-dimensional heat conduction equation, consists of a step-by-step (modular) solution to this problem by analogy with works (Togizbayeva et al., 2023).

The calculations were performed in the MATHCAD 15 environment and are shown in Figures 3–4, respectively, for a welded reinforcing plate (steel grade St3) and a modernized sidewall of the main frame of the locomotive body (for the VL-80s electric locomotive) at the installation location of the welded reinforcing plate.

An analysis of the volumetric graphical dependencies (Figures 3 and 4) reveals an increase in the values of contact thermal deformations and stresses in the sidewall of the modernized locomotive main frame (specifically, the VL80s electric locomotive) at the location of the welded-on reinforcing plate, both in its central portion and closer to the attachment points. This also corresponds to practical observations, as metal surface destruction and the accumulation of erosion cavities are observed at the welded-on reinforcing plate installation points. However, overall, the contact thermal stresses arising both in the main frame of the locomotive body sidewall and in the welded-on reinforcing plate itself are low, confirming our technology for welding reinforcing plate installations to increase strength and extend the service life of the locomotive being repaired during overhaul.

3. Results and Their Discussion

In this connection we have carried out computer calculations of $\varepsilon_k^{(1)}$ and $\varepsilon_k^{(2)}$ for the initial system (12). The

calculations were performed for various values of ν in the interval [0;0.5]. Table 1 presents the values of $\varepsilon_k^{(1)}$ and $\varepsilon_k^{(2)}$, calculated for four different at fixed $\nu = 0.25$. In the calculations 60 terms of the series were kept, which guaranteed the accuracy of the significant figure.

Table 1: The Calculations for Various Values of ν in the Interval

k	$\omega = 1$		$\omega = 0{,}5$		$\omega = 0{,}1$		$\omega = 0{,}01$	
	$\varepsilon_k^{(1)}$	$\varepsilon_k^{(2)}$	$\varepsilon_k^{(1)}$	$\varepsilon_k^{(2)}$	$\varepsilon_k^{(1)}$	$\varepsilon_k^{(2)}$	$\varepsilon_k^{(1)}$	$\varepsilon_k^{(2)}$
1	0.291	0.758	0.369	0.626	0.468	0.474	0.499	0.432
20	0.300	0.335	0.382	0.373	0.530	0.415	0.591	0.426
40	0.170	0.175	0.217	0.197	0.301	0.223	0.336	0.230
60	0.119	0.118	0.148	0.133	0.206	0.151	0.229	0.169

As one would expect, the approximations from above were given with a significant overestimation of $\varepsilon_k^{(1)}$ and $\varepsilon_k^{(2)}$.

The results obtained show that by keeping 60 terms in the systems (12) and switching to finite systems of linear algebraic equations, it is possible to organize a convergent iterative process according to Picaro's scheme using the programming environment MATHCAD 15 (Bhatti & Absamatov, 2025).

An analysis of the volumetric graphical dependencies (Figures 3 and 4) reveals an increase in the values of contact thermal deformations and stresses in the sidewall of the modernized locomotive main frame (specifically, the VL80s electric locomotive) at the location of the welded-on reinforcing plate, both in its central portion and closer to the attachment points. This also corresponds to practical observations, as surface metal destruction and the accumulation of erosion cavities are observed at the welded-on reinforcing plate installation points.

However, overall, the contact thermal stresses arising in both the main frame of the locomotive body sidewall and in the welded-on reinforcing plate itself are low, confirming our technology for welding reinforcing plate installations to increase strength and extend the service life of the locomotive being repaired during overhauls.

4. Theoretical and EXPERIMENTAL RESULTS

Based on the results of numerical calculations in the MATHCAD 15 programming environment for the modernized section of unit 1 of the bracket reinforcement on the main frame of the VL-80 electric locomotive body, it was established that the total stresses in the most loaded section do not exceed the tensile strength and are equal to σ sum = 123.71 MPa at a design speed of V_{Eq} = 110 km/h, while the tensile strength for this section 1 is equal to:

$$\mathrm{n} = \frac{[\sigma_{add}]}{\sigma\, sum} = \frac{240}{123{,}71} = 1{,}94. \tag{36}$$

The calculated safety factor was greater than 1.6, i.e., this section 1 meets the safety factor requirement.

Moreover, even if we take into account the aging of the main body frame material, when, according to formula (2), the resulting total stresses should be

$$(\sigma_y + \sigma_{ST}) \le [\sigma] = 218{,}18 \text{ MPa}, \tag{37}$$

the safety factor taking into account the aging of the material will be equal to

$$\mathrm{n}_{aging} = \frac{[\sigma]}{\sigma\, sum} = \frac{218{,}18}{123{,}71} \approx 1{,}764. \tag{38}$$

When testing the fatigue strength, it was taken into account that the main frame components of the electric locomotive body, subject to alternating asymmetric stress, require an additional safety margin due to the presence of stress concentrators and a number of other factors. At the same time, the fatigue limit is reduced by reducing the variable component of the maximum permissible stress by a factor of k_σ. The fatigue strength reduction factor for the component compared to the reference sample k_σ =2,4.

Coefficient of material sensitivity to cycle asymmetry

$$\psi_\sigma = \frac{2\sigma_T - \sigma_0}{\sigma_0} = 0{,}6, \tag{39}$$

where $\sigma_T = 200$ MPa , $\sigma_0 = 250$ MPa , $\sigma_m = 69{,}778$ MPa

At the same time, the limit of endurance

$$\sigma_{endur} = \frac{\sigma_T}{k\sigma} + \left(1 - \frac{2\sigma_T - \sigma_0}{\sigma_T k\sigma}\right)\sigma_m\,, \quad (40),$$

where according to numerical calculation $\sigma_{endur} = 131{,}36$ MPa .

Fatigue strength reserve taking into account maximum stress

$$n_\sigma = \frac{\sigma_{endur}}{\sigma_m + \sigma_{arav}} = 1{,}427, \quad (41)$$

where $\sigma_{arav} = 22{,}216$ MPa – reduced amplitude voltage, which is calculated using the formula

$$\sigma_{rav} = 2{,}17\sqrt[6]{(\sum_i R_i)}, \quad (42)$$

where R_i is the reduced amplitude stress of the calculated asymmetric cycle of dynamic loading of frame parts, calculated according to the numerical calculation in the program compiled for the MATHCAD 15 programming environment (Bhatti & Absamatov, 2025).

As a result of numerical studies on the sections of the main frame of the VL-80 electric locomotive body, it was established that, taking into account the modernization carried out by installing reinforcing linings, the fatigue strength is sufficient, since it exceeds the minimum value of 1.4.

Based on the analytical and numerical studies conducted (Avdeeva et al., 2023; S. M. Wahid & C. Madhusudana, 2000; Zhang et al., 2023) and a comparative analysis with our experimental studies (Togizbayeva et al., 2023), the following general conclusions can be drawn:

1. A generalized method for calculating the dynamic strength of frame structures of complex-configured locomotives for transport engineering has been developed, taking into account the influence of contact dynamic and thermal loads, as well as longitudinal, transverse, and torsional components of traction forces at elevated speeds, specifically for the main frame and bogie frames of the VL-80 electric locomotive (Avdeeva et al., 2023; S. M. Wahid & C. Madhusudana, 2000; Zhang et al., 2023).

2. As a result of numerical calculations performed using the MATHCAD 15 programming environment, the maximum stresses in the design modes were obtained, determining the strength of the sidewalls of the VL-80 electric locomotive body frame after reinforcement by installing reinforcing platens. The results are summarized in Table 2.

3. Figure 6 (Fig. 6) shows a graph of the change in dynamic displacements of the sections of the main frame of the body of a VL-80 electric locomotive of standard design during bending vibrations over time (in the middle of the span).

4. Based on the data in summary Table 2, the following conclusions can be drawn:

- the maximum total stress values calculated for the most unfavorable possible load combinations for the design loading conditions of the main frame of the VL-80 electric locomotive do not exceed the permissible values;
- strengthening the main frame of the body by installing reinforcing plates reduces the maximum stresses compared to the existing design by 10-15%, depending on the loading conditions.

Table 2: Maximum Stresses in the Design Modes of the Main Frame of the VL-80 Electric Locomotive After Modernization with Reinforcement by Installing Reinforcing Plates

№	Name of the Mode		Maximum Stress, MPa
1.	Weight loading		- 21,5 MPa
	Single traction	Additional Stresses	+ 49,6
2.		Total With Weight	+ 66,0
3.	Double traction	Additional Stresses	+97,5
		Total With Weight	+114,0
4.	Compression with a force of 250 t (2.5 MN) along the axis of the automatic couplings	Additional Stresses	-198,5
		Total With Weight	-211,8
5.	Tensile force 250 t (2.5 MN) along the axle of the automatic couplers	Additional Stresses	+198,5
		Total With Weight	+215,3
6.	Impact of 250 t (2.5 MN) on the automatic coupling	Additional Stresses	-174,8
		Total With Weight	-198,1
7.	250 t (2.5 MN) jerk on the automatic coupling	Additional Stresses	+174,8
		Total With Weight	+174,8

5. According to experimental data, torsional stresses in the electric locomotive body frame are very small and were not recorded by measuring equipment (Togizbayeva et al., 2023). Therefore, we did not take them into account in our calculations of dynamic strength.

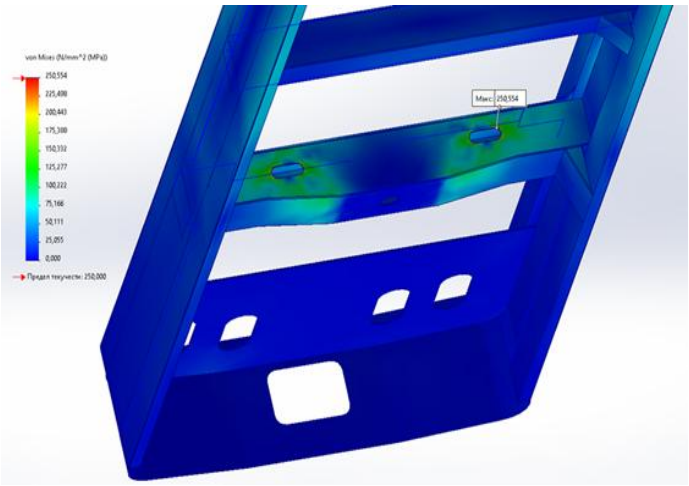

Figure 5: The Most Stressed Areas of the Electric Locomotive Frame.

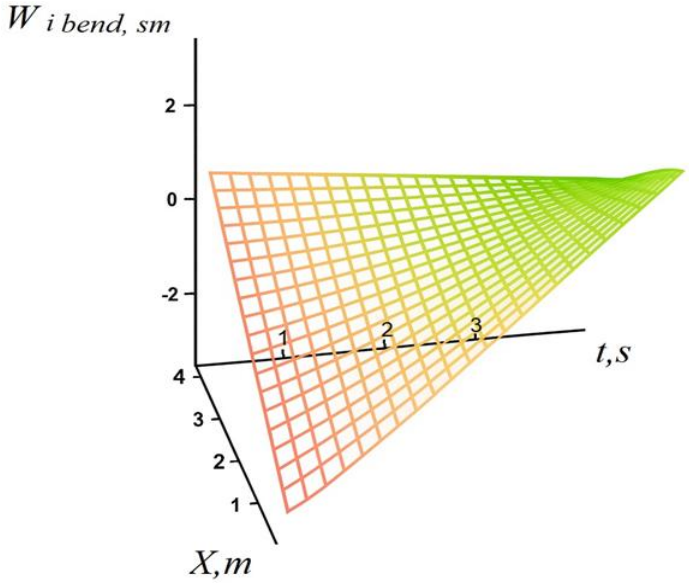

Figure 6: Graph Of Changes in Dynamic Displacements of the Sections of the Body frame of the VL-80 Electric Locomotive of Standard Design During Bending Vibrations Over Time (In The Middle Of The Span).

6. Experimental data are presented for the first time for upgraded VL80 electric locomotive body frames with the installation of reinforcing plates.

The modeling was conducted based on the characteristics of the VL80s electric locomotive main frame components obtained during measurement runs (Togizbayeva et al., 2023). During the runs, information was collected on the actual loads occurring in the VL80s electric locomotive main frame, as well as data for testing the developed onboard diagnostics algorithm under rolling stock vibration conditions.

The signals (possible diagnostic parameters) obtained during the measurements were evaluated using various algorithms as a function of time and frequency. In the first case, the statistical parameters were calculated and divided into classes; in the second case, the frequency spectra were analyzed and the transfer function was calculated. Only some of the evaluation algorithms turned out to be suitable for diagnostics.

Full-scale experimental studies on dynamic vibrations of the main body frame and bogie frames were carried out on VL80s electric locomotives.

The objectives of the experimental studies were:

1. Analysis of dynamic vibrations of the main body frame and bogie frames of the VL80s electric locomotive under operating conditions at “Uzbekistan Temir Yullari” JSC, taking into account the installation of reinforcing pads on it.

2. Determination of the prevailing frequency spectrum of oscillations and the construction of amplitude-frequency characteristics (AFC) according to the sections of the main frame of the body and frames of electric locomotive bogies. Comparison of the obtained results with theoretical calculations and known experimental studies (Avdeeva et al., 2023; S. M. Wahid & C. Madhusudana, 2000; Zhang et al., 2023).

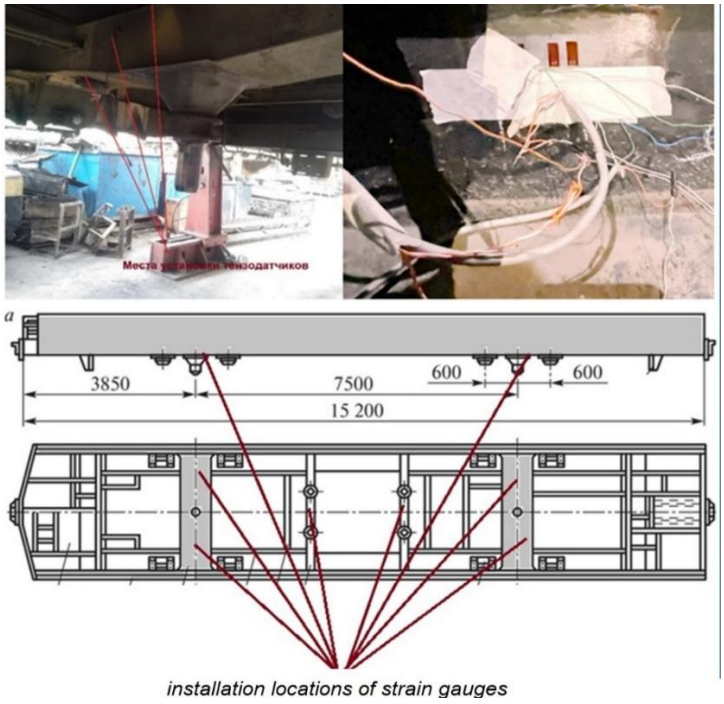

a

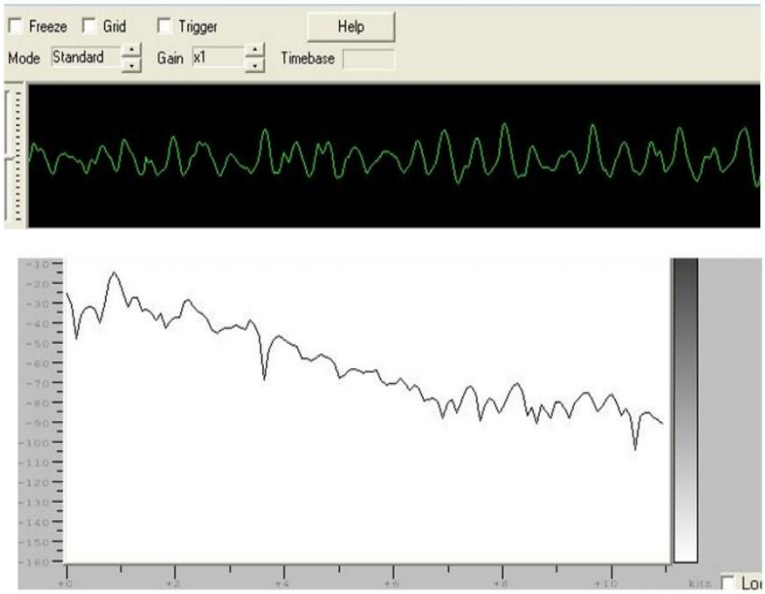

b

Figure 7: Experimental Research

a). Installation Locations of Strain Gauges on the Locomotive Frame
b). Sample Of Experimental Record: Longitudinal Stresses in the Frame of the Vl80s Electric Locomotive Bogie and Processing of the Total Frequency Spectrum.

3. Analysis of the stress-strained main frame of the body and bogie frames of the VL80s electric locomotive under various loading conditions and comparison of experimental data with theoretical data. The experiments were carried out in series with repetitions over several days. During the tests, the total time, data on the speed mode of the electric locomotive were recorded, vibrations and deformations were also recorded on the main frame of the electric locomotive body (Fig.6).

Table 3 provides generalized information about the values of vibration accelerations at various control points during the tests. Based on the interpretation of the obtained vibrograms, the main active vibration accelerations at the control points were determined.

To determine the prevailing frequencies at the control points and to analyze the vibration spectrum of the main body frame and bogie frames of the VL80 electric locomotive, standard software for personal computers in the form of "Analyzer 2022" and "Analysis Center" packages was used (Fig7).

From the spectral analysis of the obtained experimental records, it can be seen that vibrations of the main body frame and bogie frames of the VL80 electric locomotive under the influence of a driving load that occurs when the electric locomotive moves along a track with periodic unevenness and in curves experience a wide frequency spectrum of dynamic loads (from 0.1 to 5000 Hz). Vibrations with higher frequencies are also present in the spectrum, but they are not characteristic of mechanical systems and are explained by the presence of harmonic components in the spectrum.

Table 3: Information about the Conducted Experimental Measurements

Control Point	Maximum Amplitude at H338, mm	Maximum Amplitude on Monitor, dB	Vibration Acceleration, Hz	Voltage, MPa
Body Frame Vertically (Midspan)	31	66,8	2,07	Bending 68 MPa
Body Frame Horizontally (Midspan)	87,5	160	6,0	Longitudinal 38 MPa

From the analysis of the obtained experimental results it follows that the stress-strain state of the main frame parts of the VL80s electric locomotive body corresponds to known theoretical studies and practical measurements previously carried out by other researchers (Abdurasulov et al., 2025; Sethi et al., 2025; S. Wahid & C. Madhusudana, 2000).

As part of the study, a comparison of the results of a mathematical model of the frame structure of a locomotive frame of complex configuration with a model constructed using the finite element method also showed non-critical discrepancies (Table 4).

Table 4: Comparison of the Results of a Mathematical Model of the Design of a Locomotive Frame of Complex Configuration with a Model Constructed Using the Finite Element Method

№	Name of the Mode		Maximum Stress Determined by the Mathematical Model, MPa	Maximum Stress Determined by FEM, MPa	Discrepancies, %
1.	Compression with a Force of 250 t (2.5 MN) along the axis of the automatic couplings	Additional stresses	-198,5	-215,35	7.2%
		Total with weight	-211,8	-218,2	3%
2.	Tensile force 250 t (2.5 MN) along the axle of the automatic couplers	Additional stresses	+198,5	+216,3	8%
		Total with weight	+215,3	+238,3	10%

5. Conclusion

Based on the theoretical and experimental studies conducted, the following general conclusions can be drawn:

1. Computational studies to determine the actual stresses occurring in the welded seams of the main body frame

components where fatigue cracks had formed were used to select rational sizes of complex-configured reinforcing plate for the main body frame components of VL-80 electric locomotives.

2. Theoretical studies have established that the movement of a railway vehicle is accompanied by vertical vibrations of the locomotive body with a natural frequency typically of 1–2.5 Hz, while vibrations with an acceleration of (0.15–0.3) g arise due to track irregularities. Consequently, the vibration amplitude is smaller on seamless track, while it is greater on track with welds (with a rail length of 25 m and 12.5 m). The locomotive bogie also has its own natural vibration frequency—typically around 4–15 Hz, with acceleration reaching (2–3) g. As a result of system vibrations, dynamic stresses with an amplitude of up to 40 MPa arise in the bogie (Togizbayeva et al., 2023).

3. A generalized mathematical model and an analytical-numerical method have been developed for three-dimensional modeling of changes in contact temperature fields at the location of a steel plate welded to the modernized sidewall of the locomotive body's main frame.

4. The scientific novelty of the proposed numerical-analytical method lies in the development of a coupled thermomechanical model that integrates three-dimensional thermal conductivity with the theory of spatial elasticity. Unlike traditional approaches, the proposed model simultaneously takes into account thermal effects caused by welding and dynamic loads during operation, allowing for a more realistic representation of operating conditions.

An efficient computational algorithm based on Fourier-Bessel series, Laplace transforms, and iterative methods has been developed. The approach ensures stable convergence and is suitable for engineering applications, reducing computational complexity compared to full-scale numerical models.

5. Experimental validation using full-scale tests of VL80 locomotives demonstrated relatively high model prediction accuracy, with deviations within 3–10%. This confirms the reliability of the proposed methodology for practical application. The effect of structural reinforcement with welded plates was quantitatively assessed. The results show an increase in safety factors by 10–15% in critical areas while maintaining safety factors above regulatory limits (≥1.4), even under material aging conditions.

6. Thermal contact effects were found to have a moderate but significant impact on the stress-strain state. Taking them into account improves the accuracy of durability prediction, particularly in welded joints.Fatigue strength analysis confirmed the adequate durability of the modernized structures, with safety factors exceeding the minimum required values, confirming the effectiveness of the proposed modernization strategy.

8. An engineering method of analytical and numerical calculation is proposed, which enables quasi-static and dynamic modeling of the stress-strain state of the main body frame and bogie frames of locomotives with a modernized reinforced supporting framework, based on numerical calculation programs, for which two certificates of official registration of a computer program of the Republic of Uzbekistan have been received (No. DGU 07664, dated April 31, 2020, and No. DGU 10286 dated February 24, 2021).

9. In order to improve operational safety, an improved "Methodology for expert technical diagnostics of VL-80s electric locomotives in order to extend their useful life" has been developed. Its application in the modernization of locomotives during overhaul will improve their dynamic characteristics, increase the strength and reliability of the supporting structures of the electric locomotive frames. 10. A new method for modernizing locomotives during overhauls has been developed to improve dynamic performance, increase strength, reliability, and extend their useful life. Implementation of the proposed modernization method for nine 3VL80s electric locomotives resulted in an economic benefit of 678 million soums in 2022 (reference from JSC Uzbekistan Railways dated March 30, 2023, No. H/5527-19).

11. The developed tools and proposed methods for calculating modernization parameters can be widely used in the design of new electric and diesel locomotives, as well as in scheduled overhauls and overhauls of existing locomotives, including their modernization.

References

Abdurasulov, S., Zayniddinov, N., Khamidov, O., Yusufov, A., & Jamilov, S. (2025). Stress-strain state analysis of cross beam of main frame of industrial electric locomotives PE2M and PE2U. In *AIP Conference Proceedings* (Vol. 3256, pp. 060011). AIP Publishing LLC. https://doi.org/10.1063/5.0266927

Avdeeva, A., Khromova, G., & Radjibaev, D. (2023). Two-axle bogie vibration damping system with additional damping elements. In *E3S Web of Conferences* (Vol. 365, pp. 02003). EDP Sciences. https://doi.org/10.1051/e3sconf/202336502003

Bhatti, M. A., & Absamatov, A. (2025). Adoption of Business Analytics as a Data-Driven Approach to Process Optimizations in Mechanical Manufacturing Companies' Operational Performance: Moderating role of Mechanical Technology Utilization. *Reports in Mechanical Engineering*, *6*(2), 1-15. https://doi.org/10.31181/rme505

Bianchi, G., Fanelli, C., Freddi, F., Giuliani, F., & La Placa, A. (2025). Systematic review railway infrastructure monitoring: From classic techniques to predictive maintenance. *Advances in Mechanical Engineering*, *17*(1), 16878132241285631. https://doi.org/10.1177/16878132241285631

Guerrieri, M. (2023). Wheel-Rail Interaction and Derailment Analysis. In *Fundamentals of Railway Design* (pp. 79-87). Springer. https://doi.org/10.1007/978-3-031-24030-0_4

Sethi, M., Sushil, & Gupta, M. (2025). Modelling the enablers of organizational resilience: a modified total interpretive structural modeling (m-TISM) approach. *Benchmarking: An International Journal*, *32*(5), 1776-1824. https://doi.org/10.1108/BIJ-09-2023-0621

Sumbodo, W., Pambudi, R., & Setiadi, R. (2025). Design and Analysis of Pick and Place Robot Gripper in the Fertilizer Industry. *Reports in Mechanical Engineering*, *6*(2), 53-64. https://doi.org/10.31181/rme511

Togizbayeva, B., Zabiyeva, A., Balabekova, K., & Kenesbek, A. (2023). Development of a Calculation Method for Determining the Permissible Dimensions of the Defect 11. *Acta Polytechnica Hungarica*, *20*(4). https://acta.uni-obuda.hu/Togizbayeva_Zabiyeva_Balabekova_Kenesbek_133.pdf

Tulekov, A., Togizbayeva, B., Kenesbek, I., Kenesbek, A., & Zabiyeva, A. (2023). The Use of Composite Materials in the Production of Tower Cranes. *Acta Polytechnica Hungarica*, *20*(9), 277–291. https://doi.org/10.12700/APH.20.9.2023.9.16

Vasiliev, V. V., & Morozov, E. V. (2001). *Mechanics and analysis of composite materials*. Elsevier. https://shorturl.at/1X6fN

Vujanović, D., Momčilović, V., Bojović, N., & Papić, V. (2012). Evaluation of vehicle fleet maintenance management indicators by application of DEMATEL and ANP. *Expert Systems with Applications*, *39*(12), 10552-10563. https://doi.org/10.1016/j.eswa.2012.02.159

Wahid, S., & Madhusudana, C. (2000). Gap conductance in contact heat transfer. *International Journal of Heat and Mass Transfer*, *43*(24), 4483-4487. https://doi.org/10.1016/S0017-9310(00)00071-5

Wahid, S. M., & Madhusudana, C. (2000). Gap conductance in contact heat transfer. *International journal of heat and mass transfer*, *43*(24), 4483-4487. https://doi.org/10.1016/S0017-9310(00)00071-5

Yovanovich, M. (2000). Thermal-mechanical models for non-conforming surface contacts. In *ITHERM 2000. The Seventh Intersociety Conference on Thermal and Thermomechanical Phenomena in Electronic Systems (Cat. No. 00CH37069)* (Vol. 1, pp. 290-295). IEEE. https://doi.org/10.1109/ITHERM.2000.866838

Zhang, X., Lu, Y., Wang, J., Yuan, D., & Huang, X. (2023). Quantifying road transport resilience to emergencies: Evidence from China. *Sustainability*, *15*(20), 14956. https://doi.org/10.3390/su152014956